DETECTION OF CHANGES IN LAND DEGRADATION IN NORTHEAST CHINA FROM LANDSAT TM AND ASTER DATA

Jay Gao

School of Geography, Geology and Environ. Science, University of Auckland, Private Bag 92019, Auckland, New Zealand
e-mail: jg.gao@auckland.ac.nz

ThS-18 Change Detection

KEY WORDS: Remote Sensing, Change Detection, Land Degradation, Thematic Accuracy, Landsat, ASTER, China

ABSTRACT:

This study aims to determine the accuracy level at which different forms of land degradation can be mapped from medium-resolution satellite data, and to assess how accurately degraded land can be detected from multi-temporal satellite images. Land degradation in the form of salinization and waterlogging in Tongyu County, western Jilin Province of Northeast China was mapped from Landsat TM and ASTER images at 30 m using supervised classification, together with several other land covers. These land covers have been mapped at an overall accuracy of 80% from the TM image with the accuracy for individual covers ranging from 75% to 100% except settled areas. At 80.0%, the accuracy for barren land is higher than that for degraded farmland. The overall classification accuracy was achieved at 75.3% from the ASTER data. The accuracy for degraded farmland rose marginally to 76.7%. It is concluded that moderately degraded land can be mapped from both ASTER and TM data at over 75%. Severely degraded land can be mapped more accurately over 80%. Between 1989 and 2004 grassland decreased from 282.9 km² to 79.8 km² while healthy farmland increased by well over 120%. On the other hand, fallow land increased by 125.2% due to excessively high soil salinity. Besides, degraded farmland and barren land rose by 19.1% and 33.1%, respectively. Thus, inappropriate land reclamation and cultivation are blamed for soil degradation inside the study area.

1. INTRODUCTION

As one of the most common and serious environmental problems in the world, land degradation has affected two billion hectares (22.5%) of agricultural land, pasture, forest and woodland around the world (Oldeman *et al.* 1990). Around 5 to 10 million hectares of agricultural land are lost to degradation annually. Globally, land degradation causes a loss of productivity in drylands valued between US$13-28 billion a year (Yadav and Scherr 1995). It is thus very important to determine the nature, spatial extent, magnitude, distribution, and temporal behaviour of degraded land in order to come up with effective prevention and rehabilitation measures.

Due to its extensive distribution, land degradation is ideally monitored by means of remote sensing. For instance, information on vegetation cover, rain use efficiency, surface run-off and soil erosion can be derived from remotely sensed data. The combined use of such information highlights areas highly susceptible to degradation (Symeonakis and Drake, 2004). Through monitoring changes in grassland biomass production and reclamation activities, Runnstrom (2003) detected the nature and scale of land degradation in the Mu Us Sandy Land of north central China. It is also possible to study land salinization and waterlogging from remote sensing data. Space borne satellite data have shown the potential in deriving information on the nature and spatial distribution of variously degraded lands, such as salinization and waterlogging (Dwivedi, 1994). Areas affected by degradation can be identified and mapped from Landsat Thematic Mapper (TM) images (Raina *et al.*, 1993). Information on the spatial extent and distribution of salt-affected soils can be derived from Landsat multispectral scanner (MSS) data. Visual interpretation of Landsat MSS and TM images, in conjunction with ancillary information and adequate ground data, ascertained the extent and spatial distribution of salt-affected soils, water-logged areas and eroded lands (Sujatha *et al.*, 2000). Waterlogged areas can also be mapped from a 1:50,000 Landsat TM false-colour composite print. Waterlogged areas and salt-affected soils were delineated from Indian Remote Sensing Satellite (IRS)-1B Linear Imaging Self-scanning Sensor (LISS-I) and Landsat TM data via visual interpretation (Dwivedi *et al.*, 1999).

Long-term monitoring of changes in land degradation is usually accomplished by spatially comparing multi-temporal satellite images, a technique known as change detection. It involves looking for differences between two surface models that are obtained at different times. A number of change detection techniques have been devised for this purpose, such as transparency compositing, image differencing, post-classification comparison, band ratioing, and principal components analysis (Mouat *et al.*, 1993). Although image differencing and image ratioing are relatively easy to implement, these change analysis methods based on raw pixel values require selection of an appropriate set of thresholds for measuring change. These thresholds are empirically derived to differentiate changes from background variations, which is rather challenging in some cases. By comparison, post-classification change detection allows identification and mapping of amount, location and nature of differences in land covers (Rubec and Thie, 1980). Land-cover change maps derived from post-classification comparison yielded information on the spatial distribution and type of land-cover changes (Phinn and Stanford, 2001). Furthermore, post-classification comparison is the most accurate among image differencing, vegetative index differencing, selective principal components analysis (SPCA), direct multi-date unsupervised classification, post-classification change differencing and a combination of image enhancement and post-classification comparison (Mas, 1999). However, it is unknown how accurate changes detected from post-classification can be.

The purpose of this study is to determine the accuracy level at which different forms of land degradation can be mapped automatically from medium-resolution satellite data such as 30 m ASTER data. Another objective of this study is to determine how accurately degraded land can be detected from Landsat TM and ASTER data in Northeast China, an area that has suffered from various forms of land degradation.

2. STUDY AREA

Tongyu County is located in western Jilin Province, Northeast China, extending from $122^0 02'13"$ to $123^0 30'57"E$ in longitude and from $44^0 13'57"$ to $45^0 16'$ N in latitude (Figure 1). With a temperate continental monsoon climate, this area has four distinct seasons. Annual temperature averages 5.1^0C, even though extreme temperatures can range from -32^0C to 38.9^0C. Mean annual precipitation mounts to 400-500 mm, 70-80% of which fall during July-August. There is an abundant supply of solar radiation in Tongyu. It is responsible for causing evaporation to be as high as 1 500-1 900 mm per annum, which is more than three times the average annual rainfall. Such a severe water deficit is conducive to occurrence of land salinization. Tongyu has a rich agricultural resource with arable farmland and grassland standing at 1.06 ha and 0.98 ha per person, respectively.
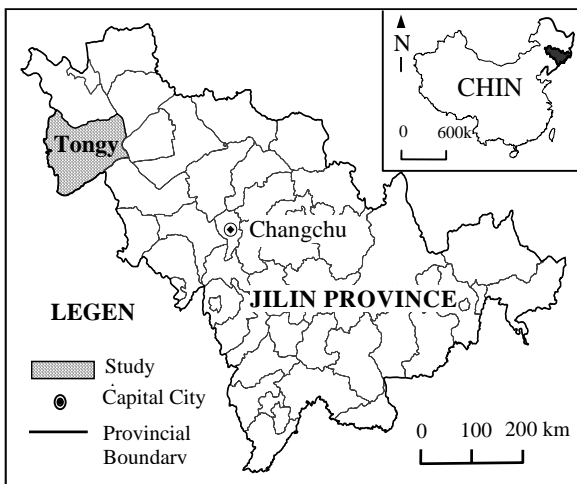
Figure 1 Location of Tongyu county in northeast China

The rich grassland and farmland resources in Tongyu make it suitable for developing farming and animal husbandry. In reality these resources have been exploited beyond their capacity. The land has been irrationally exploited in that grassland has been excessively reclaimed as farmland in direct response to population growth. Intensive grazing combined with intensive farming has led to the emergence of land degradation in the form of soil salinization and desertification. At 1.667 million ha, the saline-alkali land area in Tongyu County accounts for 32.6% of the province's total land area (Zhang and Wang, 2001). The expansion of the salinized land is driven largely by overgrazing. Land degradation has severely restricted development of regional land resources, restoration of a sound ecology and achievement of sustainable farming.

3. METHOD

3.1 Satellite Data Used

Two types of satellite data were use in this study, Landsat TM and ASTER. The full-scene Landsat TM image was acquired on 2 August 1989 (pass 120, row 29). This image has been geometrically referenced to the Universal Transverse Mercator (UTM) projection (zone 51, geodatum model: Map info) at a spatial resolution of 28.5 m. This full-scene image covers only the eastern portion of the County with little cloud coverage. A subarea (1 054 rows by 1 159 column) was delimited. Defined by two corners at (510 000, 4 970 000) and (543 003, 4 939 989.5), it covers a ground area of 32 by 30 km². Located inside this sub-area is the most severely degraded land in different forms, including salinization, alkanization, waterlogging and desertification, the first three being the most noticeable.

The ASTER data of 14 bands were recorded on 11 September 2004. These raw bands were geo-referenced to the UTM projection using 17 widely distributed ground control points (GCPs) whose coordinates were identified from the geo-referenced TM image. After eight of them were excluded from the first-order polynomial transformation, a horizontal accuracy of 0.9446 pixels was achieved for the three VNIR bands. This residual was reduced to 0.4684 pixels for the six SWIR bands, even though all the 17 GCPs were retained in the transformation. The geo-referenced VNIR and SWIR bands were output (resampled) to 30 m using the bilinear image transformation. The NVIR bands were then stacked with the SWIR ones to form a composite image, from which a ground area identical to that of the TM image was delimited. This subimage shares almost the same ground coordinates as the TM sub-image. For instance, its easting ranges from 510 000 to 543 000 and its northing from 4 970 000 to 4 940 000.

3.2 Image Classification

Prior to image classification, it was decided that land covers inside the selected area should be mapped into barren land, degraded land, productive farmland, fallow land, grassland, woodland, settled areas, wetland, and water. The same classification scheme was adopted for both Landsat TM and ASTER images except that a new category called "degraded farmland to grassland" was added to the ASTER data. Barren land refers to denuded land without any vegetative cover as a consequence of waterlogging. It represents the most severe form of land degradation. Vegetation dies completely after having been submerged underneath water for an extended period. Degraded land occurs in the form of soil salinization that has adversely affected farmland productivity. Vegetation under the influence of salinization is not so healthy and vigorous any more. Farmland falls into three categories, healthy, fallow and degraded. Healthy farmland was full of crops at the time of imaging. Fallow farmland lacked vegetative cover at the time of imaging because crops had been harvested or the land was not profitable for tilling any more. However, it is impossible to differentiate the two from the September ASTER image. Degraded farmland refers to former farmland that has been degraded to grassland. Its regular outline that is characteristic of farmland is still preserved. Grassland is the area used for grazing. Due to its fragility, grassland can be degraded very easily by overgrazing and waterlogging. Woodland refers to any bushes, shrubs, and forest. Settled areas are villages in the middle of fields. Water and wetland are areas covered by water at the time of imaging. Formed from accumulation of rainwater over shallow depressions, water bodies are seasonal lakes lack of any vegetation. Wetland represents shallow water bodies formed from enclosed paleo-channels that have been abandoned

long time ago. Distributed inside wetland are aquatic plants, such as reeds.

Training samples were selected for each of the covers in the classification scheme by delimiting polygons around areas of interest. Land covers enclosed inside these polygons were homogeneous. A completely new set of polygons were drawn from respective images. Once the derived signature was considered satisfactory, it was input into the classification

process in which the classifier was set to maximum likelihood without prior probability. The land cover maps were thematically evaluated for their accuracy before they were generalized via clumping followed by elimination at a threshold of 40 pixels or about 1 ha. The thematic accuracy of the classified maps was evaluated quantitatively. The number of evaluation pixels ranged from 20 to 40. The actual number for a given cover was proportional to its predominance in the maps.

Cover	1	2	3	4	5	6	7	8	9	Sum	Uer's Accuracy (%)
1. barren	20		3					0		**25**	80.0
2. settled	2	7	3		2			8	3	25	28
3. degraded	1		30		2		5	2		40	75
4. wetland			1	24						25	96.0
5. grassland					28			1	6	35	80.0
6. woodland				1		19				20	95
7. water							25			25	100.0
8. fallow		1			2			27		30	90
9. farmland					1			5	24	30	80.0
Sum	23	8	37	25	35	19	30	43	33	255	
Producer's Accuracy (%)	87.0	87.5	81.1	96	80	100	83.3	62.8	72.7		80.0

Table 1. Error matrix for TM (1989) image. Across: classified; down: reference (κ=0.7739)

Cover	1	2	3	4	5	6	7	8	9	10	Sum	User's Accuracy (%)
1. bare	28										**30**	93.3
2. settled		12	12					14	2		40	30.0
3. degraded	2		46	1	4	1		1	4	1	60	76.7
4. wetland		1	1	28							30	93.3
5. grassland			1	5	22	1				1	30	73.3
6. woodland			2	1	1	13		1	5	2	25	52.0
7. water		2					25				20	100.0
8. fallow			2					42	1	3	48	84.0
9. farmland			1		1			5	31	1	**40**	77.5
10. F to G*				4	1	1				24	30	80.0
Sum	30	15	65	39	29	16	25	63	43	32	350	
Producer's Accuracy (%)	93.3	80	70.8	71.8	75.9	81.3	100.0	66.7	72.1	75.0		75.3

Boldfaced figures: some of the pixels were identified as the background and thus not listed in the table
*: farmland degraded to grassland. The same below.

Table 2. Accuracy of results mapped from ASTER data at 15 m (κ=0.7221)

3.3 Change Detection
Change detection was carried out in ArcGIS by overlapping (union) the two maps. Prior to this overlay, the maps were vectorized using the raster to polygon conversion function. The overlaid map was later explored to identify the spatial changes in degraded land and the trend of land degradation.

4. RESULTS

4.1 Mapping Accuracy Achieved
Overall, the land covers have been mapped at an accuracy of 80% and a KAPPA value of 0.7739 from the 30 m Landsat TM image (Table 1). Among the user's accuracies, the lowest was achieved at 28% for settled areas due to heavy confusion with fallow farmland, degraded farmland, farmland, grassland, and even barren land. The confusion with fallow farmland and grassland is caused by the spectral similarity among these

covers that have a sparse or discontinuous vegetative cover component. Apart from this extremely low user's accuracy, however, the accuracy for all other covers is quite high, ranging from 75% for degraded farmland to 100% for water. The accuracy for degraded farmland is lowered by its mixture with four other covers. Of the 40 evaluation pixels, 5 represent water, 2 represent fallow, and 2 represent grassland. Usually, water is rarely confused with other covers thanks to its unique spectral signature and spatial uniformity. Its confusion with degraded farmland stems from the fact that vegetation submerged inside water in the rather shallow lakes and ponds is still detectable from the satellite image. At 80.0%, the accuracy for bare ground is higher than that for degraded farmland. It has been mixed with degraded land (3 out of 40 pixels), and the background (2 pixels). Unlike user's accuracies, producer's accuracies have a much narrower range from 62.8% to 100%. The highest user's accuracy was achieved for woodland whereas the lowest accuracy for fallow farmland. These percentages demonstrate

that land degradation can be mapped at a reasonable accuracy from the 30 m Landsat TM data.

The overall classification accuracy for all land covers was achieved at 75.3% from the 15 m ASTER data, slightly lower than that from the TM image (Table 2). This lower accuracy is accounted for by two factors. First, the ASTER image was recorded at a later date (11 September) than the TM image (2 August). By 11 September most crops have entered the senescence stage. This makes the accurate differentiation between non-vegetative and vegetated covers more difficult to achieve. On the other hand, all crops are still growing vigorously by 2 August. This vigour facilitates the identification of vegetative covers. Second, there is one more cover (grassland degraded from farmland) in the classification results. Mapping of more covers means that the chances of making a wrong classification are higher.

User's accuracies of the classification range from 30% to 100%. Seven of the mapped covers have a user's accuracy below 80%. The least accurately mapped covers are settled areas (30.0%) and woodland (52.0%). At 93.3%, the accuracy for bare ground is the second highest thanks to its spatial homogeneity. Only 2 out of 30 pixels were mixed with the background. The accuracy for degraded farmland is lower at 76.7%. Its confusion has occurred with farmland (4), grassland (4), barren land (2), wetland (1), grassland (1), and woodland (1). Since degraded land is either distributed with some vegetation or associated with fully covered but not so healthy vegetation, it is much more difficult to be mapped accurately than bare ground. Unlike user's accuracies, producer's accuracies are much more consistent for all covers, having a narrow range of 62.8% to 100%.

Cover	1989		2004		Change
	km²	%	km²	%	
Bare ground	39.1	4.0	58.2	5.9	+19.1
Degraded farmland	328.9	33.2	362.0	36.5	+33.1
Fallow farmland	103.1	10.4	228.3	23.0	+125.2
Healthy farmland	86.8	8.8	100.7	10.2	+13.9
Woodland	12.1	1.2	19.1	1.9	+7.0
Settled area	61.5	6.2	99.7	10.1	+38.2
Grassland	282.9	28.5	79.8	8.1	-203.1
Water	23.1	2.3	20.1	2.0	-3.0
Wetland	53.4	5.4	23.0	2.3	-30.4
Sum	990.9	100.0	990.9	100.0	0

Table 3. Mapped land covers from TM and ASTER data and their change from 1989 to 2004

Land Cover	Aster 2004									Sum
	1	2	3	4	5	6	7	8	9	
1 Degraded	219.2	36.6	12.2	10.7	10.1	2.6	24.6	4.7	5.3	
2 Barren	21.5	16.4					0.7		0.3	
3 Fallow	10.9		45.8	0.7	8.5	0.6	10.8			
4 Grassland	70.9	0.3	99.4	11.0	52.0	7.0	35.3	0.4		
5 Farmland	4.7		50.3		17.9	1.4	5.0			
6 Woodland	1.7		1.0	3.2	1.4	1.0	0.1	3.5		
7 Settled	18.2	0.8	13.4	0.6	5.2	0.7	19.5			
8 Wetland	8.1	0.2	6.1	4.1	5.4	5.5	3.2	13.9	4.0	
9 Water	6.8	4.0		0.4	0.1	0.3	0.4	0.4	10.5	
Sum	362	58.2	228.3	30.8	100.7	19.1	99.7	23.0	20.1	

*: across: land cover in 1989; down: land cover in 2004.

Table 4. Change in land covers between 1989 and 2004 (unit: km²)*

4.2 Detected Changes in Land Degradation

In 1989 the three most dominant land covers within the study site were degraded farmland (328.9 km²), grassland (282.9 km²), and fallow farmland (103.1 km²) (Table 3). They account for 72.1% of the total area (Figure 2). In 2004 the most predominant land covers were degraded farmland (362.0 km²), fallow farmland (228.3 km²), and healthy farmland (100.7 km²) (Figure 3). Significant changes occurred to grassland, farmland (both healthy and fallow), and degraded land over the study period. Grassland decreased from 282.9 km² to 79.8 km² or by over 200% while healthy farmland increased by well over 120%. These changes indicate a general trend of conversion from grassland to farmland in direct response to over population. The land was used much more intensively to produce more grains to feed the ever increasing population. Grassland was reclaimed as farmland on a massive scale. This type of change in land cover, however, may not be sustainable, as confirmed by the huge

increase (125.2%) in fallow farmland. Although some of the increased fallow farmland was due to crops being harvested by the imaging date of 11 September, it is quite possible that others were left fallow due to excessively high soil salinity. Inappropriate land reclamation and cultivation have led to soil salinization. The deteriorating degradation situation can be appreciated from the rise in degraded farmland and bare ground, which expanded by 19.1% and 33.1%, respectively.
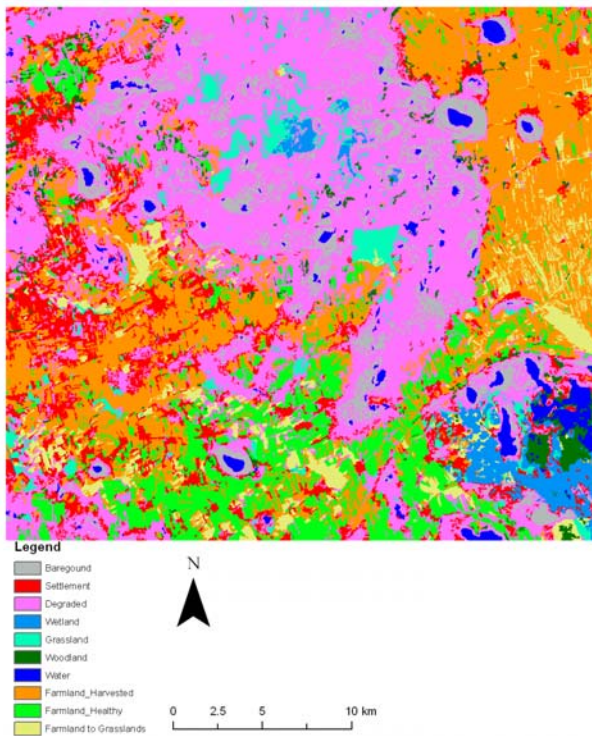
Figure 3. Land cover map produced from 15 m ASTER (2004) data.

The above discussion shows the general trend of changes among degraded lands and other covers. The specific changes among all land covers are presented in Table 4. In this table there are many minor changes valued at no more than a few square kilometres. These changes are likely to be associated with artificial errors in image classification. Thus, they are not discussed here. Instead, this discussion will focus on those major changes. Of the newly increased 36.6 lm² originated from degraded land. On the other hand, 21.5 km² barren land changed to degraded land. Another significant trend in land cover changes is the drastic rise in fallow land. The source covers for the newly increased fallow land are grassland (99.4 km²) and farmland (50.3 km²). Therefore, overgrazing has caused the land to be grazed profitably. Over cultivation has led the land to be abandoned due to the reduced productivity.

Degraded land is the cover that increased its acreage from all other covers. Among these covers, the chief ones are grassland (70.9 km²) and barren land (21.5 km²). The increase from settled areas is most likely a result of misclassification in the 1989 results. Grassland is highly vulnerable and can be degraded easily. By comparison, farmland is not easily degraded. There is also a huge change (52.0 km²) between grassland and farmland, an outcome of land reclamation.

4.3 Accuracy of Change Detection

It is very cumbersome to assess the accuracy of detected changes, a process that involves examining land covers on both images simultaneously. In order to minimize the length of assessment, it was decided to restrict the assessment to two major types of changes, from fallow farmland to degraded land, and from grassland to degraded land. A total of 30 evaluation points were selected. Checked against the ground truth as well as the original colour composite, it was found that five of the 30 points did not represent the right kind of change, resulting in an accuracy of 83.3%. The accuracy for grassland-to-degraded land was lower at 80% as changes at six of the evaluation pixels were not correctly detected.

5. CONCLUSIONS

This research has ascertained that the ASTER image of 15 m resolution produced a slightly lower overall accuracy (75.3%) than the 30 m TM image (80.0%) due to a high degree of data redundancy among its SWIR bands. However, the accuracy is comparable for degraded land, but much higher for bare ground. Therefore, ASTER data are conducive to achieving a higher mapping accuracy for severely degraded land than TM data, but has little advantage over TM data in mapping moderately degraded land.

Land cover changed on a massive scale from grassland to farmland. However, the newly reclaimed farmland may not be cultivated sustainably, as a huge amount of farmland was degraded during the same study period. The degradation situation has worsened with a rise in barren land and degraded land. Moderately degraded (e.g., salinized) land can be mapped from both ASTER and TM data at a reasonable accuracy (e.g., over 75%). Severely degraded land (e.g., barren land) caused by water-logging can be mapped at a higher accuracy of over 80%.

REFERENCES

Dwivedi, R. S., 1994, Study of salinity and waterlogging in Uttar Pradesh (India) using remote sensing data. *Land Degradation and Rehabilitation*, 5, pp. 191-199.

Dwivedi, R. S., Sreenivas, K., and Ramana, K.V., 1999, Inventory of salt-affected soils and waterlogged areas: A remote sensing approach. *International Journal of Remote Sensing*, 20, pp. 1589-1599.

Mas, J. F., 1999. Monitoring land-cover changes: A comparison of change detection techniques. *International Journal of Remote Sensing*, 20(1), pp. 139-152.

Mouat, D. A., Mahin, G. G., and Lancaster, J., 1993. Remote sensing techniques in the analysis of change detection. *Geocarto International,* 8(2), pp. 39-50.

Oldeman, R. L., Hakkeling, R. T. A., and Sombroek, W. G., 1990, World map of the status of human-induced soil degradation: an explanatory note. International Soil Reference and Information Centre, Wageningen, Netherlands.

Phinn, S., and Stanford, M., 2001. Monitoring land-cover and land-use change in a rapidly urbanising coastal environment: The Maroochy and Mooloolah Rivers catchments, southeast Queensland, 1988-1997. *Australian Geographical Studies*, 39(2), pp. 217-232.

Rubec, C. D., and Thie, J., 1980. Land use monitoring with Landsat digital data in southwestern Manitoba. ED: MacEwan, A. In Proc. 5th Canadian symposium on remote sensing, Victoria BC, August 1978. (Canadian Aeronautics and Space Institute, Ottawa), pp. 136-149.

Raina, P., Joshi, D. C., and Kolarkar, A. S., 1993, Mapping of soil degradation by using remote sensing on alluvial plain, Rajasthan, India. *Arid Soil Research and Rehabilitation*, 7, pp. 5-161.

Runnstrom, M.C., 2003, Rangeland development of the Mu Us Sandy Land in semiarid China: An analysis using Landsat and NOAA remote sensing data. *Land Degradation and Development*, 14, pp. 202.

Sujatha, G., Dwivedi, R. S., Sreenivas, K., and Venkataratnam, L., 2000, Mapping and monitoring of degraded lands in part of Jaunpur district of Uttar Pradesh using temporal spaceborne multispectral data. *International Journal of Remote Sensing*, 21, pp. 519-531.

Symeonakis, E. and Drake, N., 2004, Monitoring desertification and land degradation over sub-Saharan Africa. *International Journal of Remote Sensing*, 25, pp. 573-592.

Yadav, S. and Scherr, S., 1995, *Land Degradation in the Developing World: Is it a Threat for Food Production to the year 2020?* (Draft paper for workshop on: Land Degradation in the Developing World: Implications for Food, Agriculture and Environment to the Year 2020, 4-6 April, Annapolis, IFPRI, 190 p).

Zhang, D.F. and Wang, S.J. 2001. Mechanism of freeze-thaw action in the process of soil salinization in Northeast China. *Environmental Geology*, 41, pp. 96-100.